frontiers in Energy Research

ORIGINAL RESEARCH
published: 08 February 2021
doi: 10.3389/fenrg.2020.606494

High-Performance All-Solid-State Lithium–Sulfur Batteries Enabled by Slurry-Coated Li_6PS_5Cl/S/C Composite Electrodes

*Chao Zheng, Kai Wang, Lujie Li, Hui Huang, Chu Liang, Yongping Gan, Xinping He, Wenkui Zhang and Jun Zhang**

College of Materials Science and Engineering, Zhejiang University of Technology, Hangzhou, China

Among many lithium secondary batteries, lithium–sulfur batteries stand out because of their high theoretical specific energy, low cost, non-toxicity and the fact that they cause no environmental pollution. However, due to poor electronic and ionic conductivity, shuttle effect, lithium dendrites and other defects, it remains a big challenge to achieve large-scale application of lithium-sulfur batteries. Here we report an all-solid-state lithium–sulfur battery based on Li-argyrodite Li_6PS_5Cl solid-state electrolytes through a slurry-coating method. Li_6PS_5Cl with a high ionic conductivity of 1.3×10^{-3} S cm^{-1} at room temperature is used as the solid electrolyte and the ion conductive additive in the electrode. The sulfur-based composite cathode is fabricated through a slurry-coating process by dispersing sulfur, Li_6PS_5Cl, ethyl cellulose, and carbon black in 1,3-dioxolane (DOL). This method can disperse the Li_6PS_5Cl around sulfur particles well, and the solvent does not react with any component of composite cathodes during preparation. The battery delivers a high discharge capacity of 962 mA h g^{-1} at room temperature for the first cycle at 80 mA g^{-1}. While the Coulombic efficiency is approximately 99.5% during 100 cycles. This work provides a new insight into the combination method between the sulfide-type SSEs and sulfur cathodes, which is critical to the electrochemical performance of all-solid-state lithium-sulfur batteries.

Keywords: lithium-sulfur batteries, all-solid-state batteries, Li6PS5Cl, slurry-coating, lithium metal anode

OPEN ACCESS

Edited by:
Jiarui He,
University of Texas at Austin,
United States

Reviewed by:
Huan Pang,
Yangzhou University, China
Xiulin Fan,
Zhejiang University, China

****Correspondence:***
Jun Zhang
zhangjun@zjut.edu.cn

Specialty section:
This article was submitted to Electrochemical Energy Conversion and Storage, a section of the journal Frontiers in Energy Research

Received: *15 September 2020*
Accepted: *31 December 2020*
Published: *08 February 2021*

Citation:
Zheng C, Wang K, Li L, Huang H, Liang C, Gan Y, He X, Zhang W and Zhang J (2021) High-Performance All-Solid-State Lithium–Sulfur Batteries Enabled by Slurry-Coated Li_6PS_5Cl/S/C Composite Electrodes. Front. Energy Res. 8:606494. doi: 10.3389/fenrg.2020.606494

INTRODUCTION

With the rapid increase in the energy requirements for energy storage devices, it has been difficult to meet these needs using traditional lithium-ion batteries (LIBs) due to low energy density, poor cycle stability, and high cost. In the future, energy devices will require higher and higher energy density (Armand and Tarascon, 2008; Nitta et al., 2015; Liu et al., 2018; Wang et al., 2018b). When lithium metal (low density and high electronegativity) is paired with elemental sulfur (theoretical capacity of up to 1,672 mA h g^{-1}) to form a lithium-sulfur battery, the theoretical capacity density of the battery can reach 2600 W h kg^{-1} or 2800 W h L^{-1} (Ji et al., 2009; Yin et al., 2013). Moreover, compared with traditional LIBs, lithium-sulfur batteries have many unmatched advantages, such as being low cost, non-toxic, causes no environmental pollution and has a safer working voltage (Lochala et al., 2017; Qu et al., 2018). Based on the above advantages, lithium-sulfur batteries are regarded as the most promising next-generation energy storage product. However, there are still some bottlenecks in the

application of lithium-sulfur batteries: 1) Liquid electrolytes are easy to flow, and flammable; 2) Sulfur is an insulator, and its poor conductivity and low active material utilization seriously affect the battery rate performance; 3) Polysulfide is easily dissolved in the electrolyte and the polysulfide shuttle effects lead to poor Coulombic efficiency and cycle performance; 4) Lithium dendrites can pierce the separator, causing short circuits (Balakumar and Kalaiselvi, 2015; Pang et al., 2016; Chen et al., 2018b).

Aiming to solve the problems mentioned above, many studies mainly focus on the optimization of the electrode. Currently, the most common solution is to combine carbon materials (mesoporous carbon (Ji et al., 2009; Han et al., 2020), hollow porous carbon (Jayaprakash et al., 2011), carbon nanotube (Guo et al., 2011; Zheng et al., 2019), and graphene (Wang et al., 2011; Liu et al., 2020), etc.) with sulfur to improve sulfur utilization and to fix the polysulfide. But the surface of the carbon material is non-polar, it therefore cannot exert a strong anchoring effect on the polar polysulfide. In addition to carbon materials, metal oxides (TiO_2 (Wei Seh et al., 2013), MnO_2 (Liang et al., 2015), Al_2O_3 (Han et al., 2013), Fe_2O_3 (Zheng et al., 2017), and V_2O_5 (Carter et al., 2017), etc.) can also fix polysulfide and conductive polymers (polyaniline (PANI) (Liu et al., 2015), and polypyrrole (PPy) (Zhang et al., 2016; Geng et al., 2019), etc.) can improve electronic conductivity of composite sulfur electrodes. The low electronic conductivity of metal oxides and the high cost of conductive polymers are still not optimal solutions to the serious capacity decay during cycling for a lithium-sulfur battery. Replacing the liquid electrolyte with solid-state electrolytes to achieve an all-solid-state lithium-sulfur battery is one of the most promising strategies to solve these issues (Lin et al., 2013; Han et al., 2016a; Zhang et al., 2017; Fan et al., 2018; Zhang et al., 2018b). The conversion of sulfur does not generate soluble polysulfide, so it can fundamentally solve the polysulfide shuttle effect (Yan et al., 2019). At the same time, the ultra-high mechanical modulus of SSEs can also effectively inhibit the growth of lithium dendrites, thereby improving the Coulombic efficiency and safety of the battery (Chen et al., 2018a; Cheng et al., 2019; Shen et al., 2019; Zhao et al., 2020). Unlike traditional lithium-sulfur batteries that rely on the infiltration of liquid electrolytes to achieve rapid ion migration, in the all-solid-state lithium-sulfur batteries, the ion migration is mainly achieved through solid electrolytes (Kato et al., 2016; Yan et al., 2019; Zhao et al., 2019; Bai et al., 2020; Ding et al., 2020).

Among various SSEs, sulfide SSEs stand out because of their high ionic conductivity, low grain boundary resistance, compatible interface with sulfur-based cathodes, and their easy processability (Chen et al., 2018a; Ma et al., 2018). The most well-studied sulfide SSEs are the binary $x$$Li_2S$-(100-$x$)$P_2S_5$ system (x = 0.4–0.8) (Zhang and Kennedy, 1990; Kanno and Murayama, 2001; Ohtomo et al., 2013). The ionic conductivity of β-Li_3PS_4 synthesized *via* wet-chemistry is 1.6×10^{-4} S cm^{-1} with an activation energy of 0.36 eV (Liu et al., 2013). Crystalline $Li_7P_3S_{11}$ is also an important member of the binary system, because of its very high ionic conductivity (1.7×10^{-2} S cm^{-1} at room temperature (RT)) (Seino et al., 2014). In 2011, $Li_{10}GeP_2S_{12}$ (LGPS) was found to have a an extremely high ionic conductivity of 1.2×10^{-2} S cm^{-1} at RT (Kamaya et al., 2011). As an isostructural alternative to LGPS, $Li_{10}SnP_2S_{12}$ has the advantages of being low cost and easily promoted, but it shows a lower ionic conductivity of 4×10^{-3} S cm^{-1}, because of a slightly different lithium ion disorder (Bron et al., 2013). The highest reported ionic conductivity was found in the doping binary system, $Li_{9.54}Si_{1.74}P_{1.44}S_{11.7}Cl_{0.3}$, 2.5×10^{-2} S cm^{-1} at RT (Kato et al., 2016). Li-argyrodite Li_6PS_5Cl was reported as a promising electrolyte with a high ionic conductivity of 1.3×10^{-3} S cm^{-1} at RT (Boulineau et al., 2012; Zhang et al., 2018a; Zhang et al., 2019). The disadvantages of most sulfide electrolytes are their narrow electrochemical window and the electrochemical instability between the electrolytes and lithium metal (Han et al., 2016b). The theoretical calculation results (Zhu et al., 2015; Han et al., 2016b; Zhu et al., 2016) show that LGPS begins to be lithiated and reduced at 1.7 V. The phase equilibrium components of LGPS at 0 V consist of Li_3P, Li_2S, and $Li_{15}G_4$, which have also been observed in experiments. The interphase has a higher growth rate between LGPS and lithium, which means the presence of cations in SSEs such as Ge, Sn, Ti is detrimental to the formation of stable interface (Sakuma et al., 2016). But Li_6PS_5Cl can form a stable SEI, the thickness of SEI and interfacial resistance become stable after a certain time and no longer increase over time (Wenzel et al., 2016a; Wenzel et al., 2016b; Wenzel et al., 2018). Many cathode active materials such as $LiCoO_2$, $LiNi_{0.8}Co_{0.1}Mn_{0.1}O_2$, S, and Li_2S have been used in all-solid-state lithium batteries (ASSLBs) with Li_6PS_5Cl (Boulineau et al., 2012; Boulineau et al., 2013; Huang et al., 2015; Yubuchi et al., 2015; Han et al., 2016a; Yu et al., 2016; Zhang et al., 2018a; Zhao et al., 2019; Zhang et al., 2020). Han et al. used a novel bottom-up method to synthesize nanocomposite cathode by dissolving Li_2S and Li_6PS_5Cl in ethanol, which showed a large reversible capacity of 830 mAh g^{-1} at 50 mA g^{-1} for 60 cycles (Han et al., 2016a). Yu et al. fabricated the S/Li_6PS_5Cl/Li-In ASSLBs with a ball-milled S-Li_6PS_5Cl composite cathode (Yu et al., 2016). The batteries displayed large capacity around 1,400 mAh g^{-1} during the first cycle and decayed rapidly 400 mA h g^{-1} after 20 cycles. In 2018, Nan et al. employed the nano-sulfur/multiwall carbon nanotube composites combined with Li_6PS_5Cl as the cathode, which delivered a high discharge capacity of 1850 mA h g^{-1} at 0.1 C for the first cycle and 1,393 mAh g^{-1} after 50 cycles (Wang et al., 2018a).

However, there are very few works on the synthesis of sulfur composite cathodes for ASSLBs by wet chemical methods. In this work, we proposed a new preparation method about sulfur-composite electrodes for ASSLBs using a liquid-phase process with a DOL solution. The sulfur-composite electrodes consist of sulfur as the active material, Li_6PS_5Cl as the solid electrolyte, ethyl cellulose as the binder, and Super P (SP) as the conductive additive. The microstructure, ionic and electronic conductivity, and electrochemical stability of Li_6PS_5Cl were systematically investigated. The electrochemical property of the sandwich-type S/Li_6PS_5Cl/Li cell was tested at 80 mA g^{-1} and 30 °C. Finally, to further investigate how interface affects battery performance, S/Li_6PS_5Cl interface properties before and after cycling were examined by *ex situ* characterizations including scanning electron microscopy (SEM), energy-dispersive spectra (EDS), and electrochemical impedance spectra (EIS).

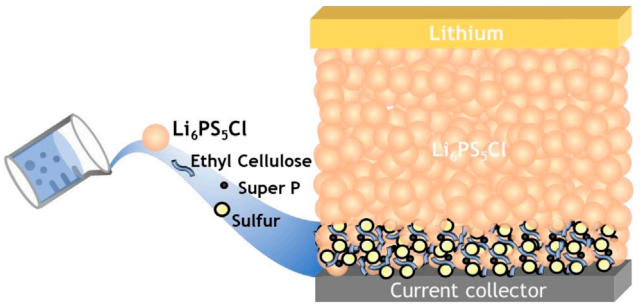

FIGURE 1 | Schematic diagram of the slurry Li_6PS_5Cl-coated sulfur-composite electrode and S/Li_6PS_5Cl/Li ASSLBs.

EXPERIMENTAL SECTION

Material Synthesis

Synthesis of Li_6PS_5Cl: The Li_6PS_5Cl was prepared using a method described in our previous work (Zhang et al., 2018a; Zhang et al., 2019; Zhang et al., 2020). In brief, a stoichiometric mixture of laboratory-grade Li_2S, P_2S_5 (99%, Aladdin), and LiCl (99.99%, Aladdin) was milled at 500 rpm for 24 h. Subsequently, the mixture was sealed in a stainless-steel tube and annealed at 500 °C for 2 h to obtain argyrodite Li_6PS_5Cl. All the experiments were carried out in an Ar-filled glove box (H_2O and O_2 < 0.5 ppm).

Fabrication of All-Solid-State Lithium-Sulfur Batteries

The sulfur-composite electrodes (sulfur powder (99%, Alfa Aesar): Li_6PS_5Cl: SP (SCM industrial Chemical Co., Ltd.): ethyl cellulose (Aladdin)) were dispersed with anhydrous DOL (≥99.8%, Aladdin) in a mass ratio of 60 : 25: 10 : 5 under continuous stirring for 6 h. The slurry was then coated onto carbon-coated aluminum foil with a glass rod and dried at 55°C for 24 h. The average sulfur loading in each electrode is 0.95 mg cm^{-2}. For the assembly of S/Li_6PS_5Cl/Li cell, the sulfur-composite electrode was covered with 120 mg Li_6PS_5Cl powder and pressed together under 350 MPa in a stainless-steel tank with a diameter of 12 mm. After that, lithium metal as the counter electrode was attached on the other side of the Li_6PS_5Cl layer. Finally, three-layered pellets (shown in **Figure 1**) were assembled with a 2032 coin-type cell in an Ar-filled glove box. For the SS/Li_6PS_5Cl/Li, Li/Li_6PS_5Cl/Li cell and SS/Li_6PS_5Cl/SS, lithium foil or stainless steel (SS) as the working electrode, the assembling procedure remained exactly the same. All the procedures were carried out in an Ar-filled glove box (H_2O and O_2 < 0.5 ppm).

Characterization and Electrochemical Measurements

X-ray diffraction (XRD) patterns of samples were recorded by an X-ray diffractometer (Rigaku Ultima IV) with Cu K_α radiation (λ = 0.15418 nm). Data was recorded in the 2-theta range of 10–80°. The Raman spectra in a range of 100–2,500 cm^{-1} were collected using a DXR Raman microscope (Renishaw InVia Raman spectrometer) with He-Ne 532 nm laser excitation and a ×50 objective. The laser beam with a laser spot size of *ca.* 1 μm was focused on each sample and the acquisition time for each spectrum was 20 s. The morphology of samples was observed by SEM (SEM, Hitachi S4700). An elemental analysis was conducted on EDS attached to SEM. The cyclic voltammetry (CV) measurement, the linear sweep voltammetry (LSV) measurement, and the direct-current (DC) polarization test was conducted on a CHI660D electrochemical workstation (Chenhua, Shanghai). The CV curve of S/Li_6PS_5Cl/Li cell was recorded between 0.4 V and 3 V with a sweep rate of 0.1 mV s^{-1}. The LSV curve of SS/Li_6PS_5Cl/Li cell was recorded in the potential range from 0 to 6 V with a sweep rate of 0.1 mV s^{-1}. DC polarization test of a blocking SS/Li_6PS_5Cl/SS cell at 2 V to determine the electronic conductivity. The ionic conductivity of Li_6PS_5Cl was calculated by the equation:

$$\sigma = \frac{d}{S \times R} \tag{1}$$

where R is the total resistance of the electrolyte, d is the sample thickness, and S is the area of the electrolyte. The total resistance of Li_6PS_5Cl was measured on the SS/Li_6PS_5Cl/SS cell using the Zennium electrochemical workstation (ZAHNER, Germany), in which the frequency ranges from 100 mHz to 4 MHz with an amplitude of 10 mV and the testing temperature ranges from 25 °C to 60 °C in stepwise increments of 5 °C. The EIS measurements of the S/Li_6PS_5Cl/Li cell before and after the cycle were measured using the same instrument in the same frequency. A Galvanostatic discharge-charge test of S/Li_6PS_5Cl/Li cell was performed in a potential range from 0.4 to 3 V (*vs.* Li^+/Li) at 80 mA g^{-1} using a Neware battery test system (Neware, Shenzhen). The stability of lithium against Li_6PS_5Cl was tested by the Neware using symmetric Li/Li_6PS_5Cl/Li cell at a current density of 0.1 mA cm^{-2}.

RESULT AND DISCUSSION

The crystal structure, composition, and morphology of the sulfur-composite electrode were characterized by XRD, Raman, and SEM, respectively. **Figure 2A** shows the typical XRD patterns of the sulfur-composite electrode and all the materials used in the synthesis process. After sintering at 500 °C for 2 h, the peaks of Li_6PS_5Cl can be indexed to the crystalline Li_7PS_6 structure, where the Cl atoms can replace S atoms in Li_7PS_6 (Deiseroth et al., 2008). Regarding the sulfur-composite electrode, there are no obvious peaks of sulfur; the main diffraction peaks and the broad diffraction peaks are indexed as Li_6PS_5Cl and amorphous carbon materials with low crystallization degree, respectively. It indicates that Li_6PS_5Cl can distribute evenly on the surface of sulfur particles. By comparing the Raman spectra (**Figure 2B**) of all materials, the sulfur-composite electrode can be further analyzed. The weak peak at 425 cm^{-1} associated with PS_4^{3-} (*ortho-*

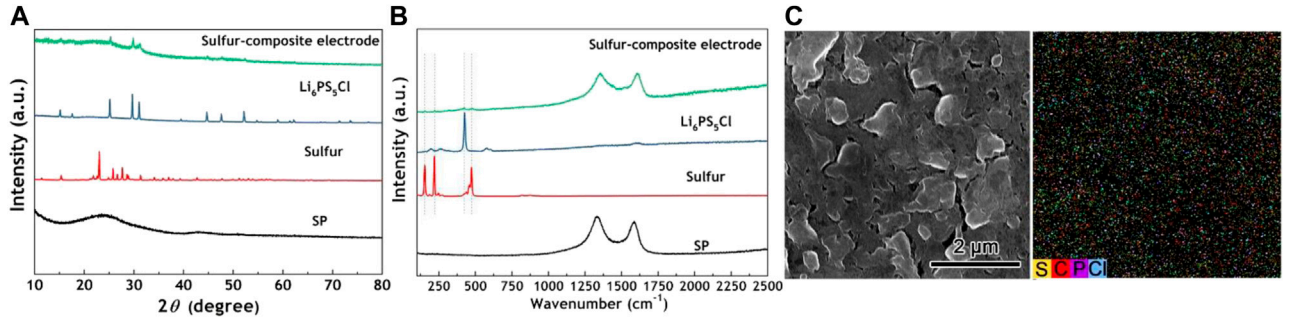

FIGURE 2 | (A) XRD patterns and **(B)** Raman spectra of the conductive additives (SP), sulfur, Li_6PS_5Cl, sulfur-composite electrode **(C)** The SEM image and corresponding elemental mappings of sulfur-composite electrode.

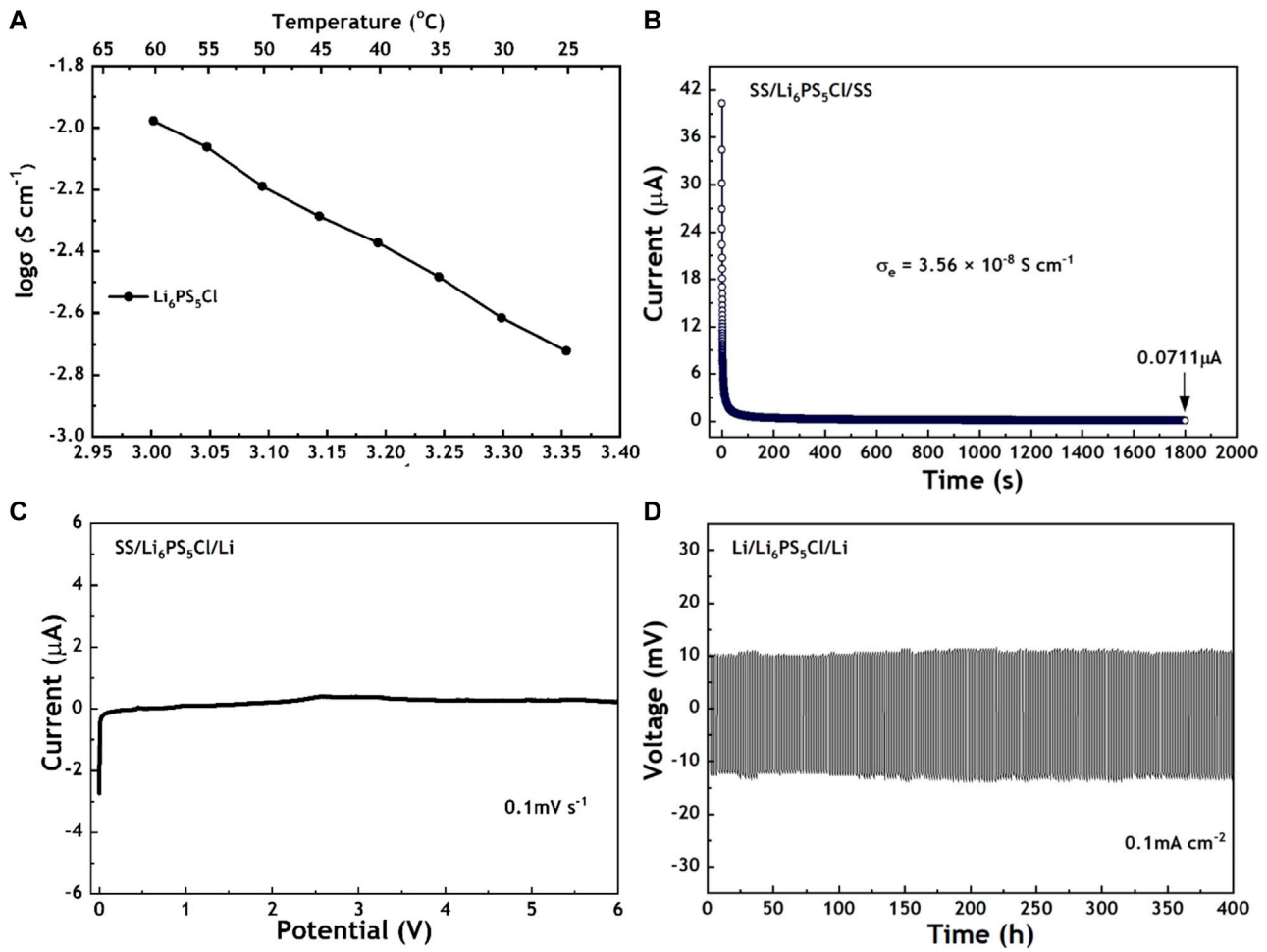

FIGURE 3 | (A) Temperature dependence of the ionic conductivity of Li_6PS_5Cl **(B)** DC polarization of a blocking SS/Li_6PS_5Cl/SS cell **(C)** LSV curve of the SS/Li_6PS_5Cl/Li cell **(D)** Voltage profile of the symmetric Li/Li_6PS_5Cl/Li cell at 0.1 mA cm^{-2}.

thiophosphate) from the ionic formula $(Li^+)_6(PS_4^{3-})S^{2-}Cl^-$ (Deiseroth et al., 2008; Ohara et al., 2016) and peaks at 153 cm^{-1}, 219 cm^{-1} and 474 cm^{-1} associated with S–S bond were observed, indicating no chemical reaction occurred in DOL solvent during the synthesis process. As shown in **Supplementary Figure S1**, the irregular shape of the Li_6PS_5Cl particle is beneficial to increasing the contact area between the active material and electrolyte in the composite cathode. As seen

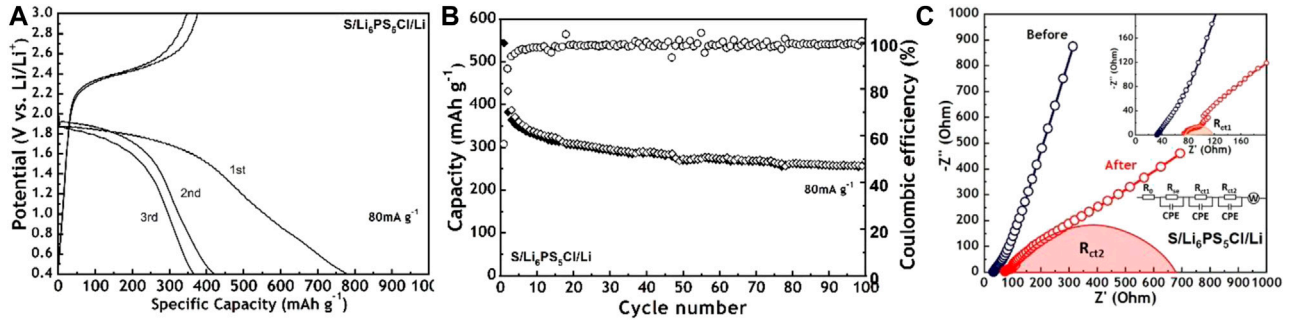

FIGURE 4 | (A) Charge-discharge profiles during the first threes cycles and **(B)** cycling performance of S/Li_6PS_5Cl/Li cell at 80 mA g^{-1} and 30°C **(C)** Nyquist plots of S/Li_6PS_5Cl/Li cell before cycling and after 100 cycles at 80 mA g^{-1}.

from the morphology and elemental distribution in **Figure 2C**, the sulfur particles are well embedded in the solid electrolyte and conductive additives, resulting in a dense composite and a low interfacial resistance.

The temperature dependence of the ionic conductivity of Li_6PS_5Cl was systematically investigated. **Supplementary Figure S2** shows the different impedance spectra of Li_6PS_5Cl at different temperatures. Through calculations based on resistance values, the ionic conductivity of Li_6PS_5Cl exhibits a gradual increase as the temperature increases, as shown in **Figure 3A**. It shows the ionic conductivities of 1.30×10^{-3} S cm^{-1} and 1.05×10^{-2} S cm^{-1} at 25 °C and 60 °C, respectively. The activation energy E_a is calculated from the slope of the linear Arrhenius plot according to the Arrhenius equation:

$$\sigma(T) = A \times e^{\left(-\frac{E_a}{k \times T}\right)}, \quad (2)$$

where T is the absolute temperature, A is a pre-exponential factor, and k is the Boltzmann constant. According to **Figure 3A**, the E_a value of Li_6PS_5Cl is 0.32 eV, which is low in comparison to most sulfide SSEs. In addition to ionic conductivity, the electronic conductivity of Li_6PS_5Cl has also been investigated by the DC polarization test (**Figure 3B**). It shows a low electronic conductivity of 3.56×10^{-8} S cm^{-1}, which is beneficial for suppressing lithium dendrite growth. LSV was used to determine the electrochemical window, which is important in evaluating the stability of Li_6PS_5Cl against a lithium anode and cathode. As shown in **Figure 3C**, the decomposition current corresponding to Li stripping ($Li \rightarrow Li^+ + e^-$) is observed around 0 V vs Li/Li^+. There is no significant current change in the potential range from 0 to 6 V vs Li/Li^+. Assembling the symmetric Li/Li_6PS_5Cl/Li cell is also an important experimental method to investigate the stability between Li_6PS_5Cl and lithium. The voltage profile of Li_6PS_5Cl remains at a lower voltage (≈10mV) during 400 h at 0.1 mA cm^{-2}. The results of LSV and symmetric battery prove that the Li_6PS_5Cl is suitable to pair with the lithium anode. Considering the high ionic conductivity, low electronic conductivity, and wide electrochemical window, Li_6PS_5Cl is an appropriate candidate for an ionic conductor and battery separator.

Figure 4A shows the charge-discharge profiles of the S/Li6PS5Cl/Li cell between 0.4 and 3.0 V during the first three cycles. The current density is 80 mA g-1 and the test temperature is 30 °C. The initial discharge capacity of ASSLBs is 962 mAh g-1 and the corresponding Coulombic efficiency is as low as 56%, which are ascribed to the activation process for the sulfur cathode, interfacial decomposition, and the interfacial chemical reaction between the electrolyte and electrode (Zhang et al., 2015; Han et al., 2016a). As shown in **Supplementary Figure S3**, the CV was used to study the mechanism of the electrode reaction. During the first cycle, one reduction peak can be observed at 1.8 V due to the reduction of S to Li2S and the oxidation peak at 2.5 V can be attributed to the oxidation of Li2S to S (Takeuchi et al., 2010; Wang et al., 2018a). During the subsequent cycles, both reduction and oxidation peaks slightly shift, which means a good reversibility of the composite cathode. **Figure 4B** presents the cycling performance and Coulombic efficiency, the cell delivers a high Coulombic efficiency of nearly 100% after three cycles, specific capacity decreases to 387 mAh g-1, and capacity retention reaches 66% after 100 cycles. The impedance changes for the S/Li6PS5Cl/Li cell before and after cycling are shown in **Figure 4C**. Two Nyquist plots were fitted into one equivalent circuit. The equivalent circuit is constructed to distinguish common resistances: Rse, Rct1, Rct2, and Zw, representing the bulk resistance, two interfacial resistances, and Warburg impedance, respectively (Deng et al., 2015; Takada et al., 2015). Based on our previous work (Zhang et al., 2020), the Rct1 and Rct2 represent the interfacial resistance between lithium and the electrolyte, and the interfacial resistance between the cathode and electrolyte, respectively. The bulk and interfacial resistance values increase after cycling. But the variations of Rse and Rct1 are very small (≈40 Ω). There is a large difference in value (≈675 Ω) of Rct2, which is attributed to interfacial reactions or a chemo-mechanical failure (Ohno et al., 2019). These negative effects may be the main reason for the low initial Coulombic efficiency and the subsequent capacity loss.

To investigate the interfacial reactions or chemo-mechanical failure in the S/Li_6PS_5Cl/Li cell after cycling, a cross-sectional SEM was conducted, and the elemental distributions of Al, S, P, Cl, and C elements in the red selected area were assessed by EDS,

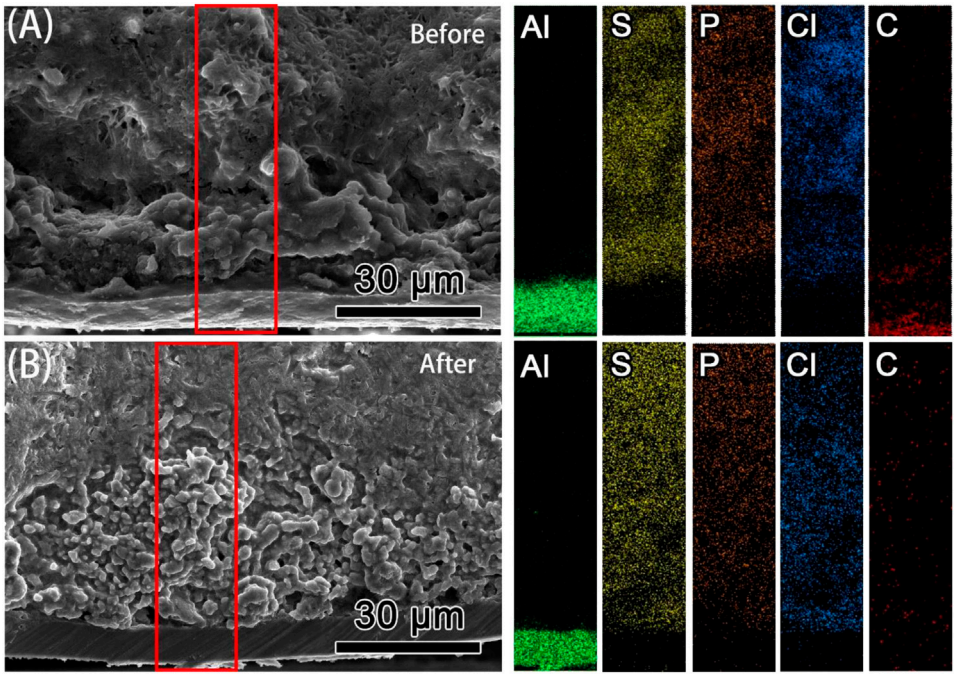

FIGURE 5 | The cross-sectional SEM images and the corresponding elemental mappings of the interface between Li_6PS_5Cl and sulfur-composite electrode **(A)** before cycling and after **(B)** 100 cycles at 80 mA g^{-1}.

as depicted in **Figure 5**. Since both active material and electrolytes are sulfur-based materials, it is difficult to determine where the chemical decomposition products at the interface come from. Compared to the morphologies and elemental distribution of the C element at the S/Li_6PS_5Cl interface, it was found that the thickness of the sulfur-composite electrode after cycling is more than twice what it was before. This significant change can be explained by the volume change (chemo-mechanical failure) because of the conversion reaction of S and a small number of Li_6PS_5Cl. There is about 80% added volume in the cathode after discharging, when 1 mole of S_8 converted into 8 moles of Li_2S. The loose distribution of the C element after cycling, confirms that the volume increase stresses the surrounding matrix of solid electrolytes and carbon materials, resulting in a lot of pores and voids in the cathode. Thus, at this scale, such a large volume change has a much greater impact on interfacial resistance than on chemical reactions. In other words, chemo-mechanical failure is an urgent issue that needs to be resolved in all-solid-state lithium-sulfur batteries.

CONCLUSION

Argyrodite Li_6PS_5Cl is an ionic conductor with high ionic conductivity and a wide electrochemical window. The Li_6PS_5Cl possesses good potential for applications in lithium-sulfur batteries. We successfully demonstrated a new strategy to fabricate a sulfur cathode for ASSLBs *via* the solution coating method by mixing sulfur materials, Li_6PS_5Cl solid electrolyte, ethyl cellulose binder, and SP conductive additive in a DOL solution. The slurry coating achieved intimate contact between the S/C particles and the Li_6PS_5Cl solid electrolyte, guaranteeing adequate lithium-ion pathways. The battery shows a high initial discharge capacity of 962 mAh g^{-1} at 80 mA g^{-1} and a specific capacity of 387 mAh g^{-1}. After 100 cycles, the capacity retention reaches 66%. Although the Li_6PS_5Cl solid electrolyte can eliminate the shuttle effect and alleviate interfacial reaction, the volume change of sulfur still seriously affects the performance of ASSLBs.

DATA AVAILABILITY STATEMENT

The raw data supporting the conclusions of this article will be made available by the authors, without undue reservation.

AUHTOR CONTRIBUTIONS

Conceptualization, JZ, HH, and WK; experimental, CZ, KW, and LL; data analysis, CZ, YG, YX, and CL; writing—original draft preparation, ZC; writing—review and editing, JZ; supervision, JZ, and WZ. All authors have read and agreed to the submitted version of the manuscript.

FUNDING

The authors acknowledge the support of the Zhejiang Provincial Natural Science Foundation of China under grant No.

LR20E020002, the National Natural Science Foundation of China (NSFC) under grant No. 21972127, 51677170, 51777194, and 51722210, the China Postdoctoral Science Foundation under grant No. 2020M671786 and the Zhejiang Xinmiao Talents Program No. 2020R403086.

SUPPLEMENTARY MATERIAL

The Supplementary Material for this article can be found online at: https://www.frontiersin.org/articles/10.3389/fenrg.2020.606494/full#supplementary-material.

REFERENCES

Armand, M., and Tarascon, J. M. (2008). Building better batteries. *Nature* 451 (7179), 652–657. doi:10.1038/451652a

Bai, Y., Zhao, Y., Li, W., Meng, L., Bai, Y., and Chen, G. (2020). Organic-inorganic muldslti-scale enhanced interfacial engineering of sulfide solid electrolyte in Li-S battery. *Chem. Eng. J.* 396, 125334. doi:10.1016/j.cej.2020.125334

Balakumar, K., and Kalaiselvi, N. (2015). High sulfur loaded carbon aerogel cathode for lithium-sulfur batteries. *RSC Adv.* 5 (43), 34008–34018. doi:10.1039/C5RA01436K

Boulineau, S., Courty, M., Tarascon, J.-M., and Viallet, V. (2012). Mechanochemical synthesis of Li-argyrodite Li6PS5X (X=Cl, Br, I) as sulfur-based solid electrolytes for all solid state batteries application. *Solid State Ionics* 221, 1–5. doi:10.1016/j.ssi.2012.06.008

Boulineau, S., Tarascon, J.-M., Leriche, J.-B., and Viallet, V. (2013). Electrochemical properties of all-solid-state lithium secondary batteries using Li-argyrodite Li6PS5Cl as solid electrolyte. *Solid State Ionics* 242, 45–48. doi:10.1016/j.ssi.2013.04.012

Bron, P., Johansson, S., Zick, K., Schmedt auf der Günne, J., Dehnen, S., and Roling, B. (2013). Li10SnP2S12: an affordable lithium superionic conductor. *J. Am. Chem. Soc.* 135 (42), 15694–15697. doi:10.1021/ja407393y

Carter, R., Oakes, L., Muralidharan, N., Cohn, A. P., Douglas, A., and Pint, C. L. (2017). Polysulfide anchoring mechanism revealed by atomic layer deposition of V2O5 and sulfur-filled carbon nanotubes for lithium-sulfur batteries. *ACS Appl. Mater. Interfaces* 9 (8), 7185–7192. doi:10.1021/acsami.6b16155

Chen, S., Xie, D., Liu, G., Mwizerwa, J. P., Zhang, Q., Zhao, Y., et al. (2018a). Sulfide solid electrolytes for all-solid-state lithium batteries: structure, conductivity, stability and application. *Energy Storage Materials* 14, 58–74. doi:10.1016/j.ensm.2018.02.020

Chen, W., Lei, T., Wu, C., Deng, M., Gong, C., Hu, K., et al. (2018b). Designing safe electrolyte systems for a high-stability lithium-sulfur battery. *Adv. Energy Mater.* 8 (10), 1702348. doi:10.1002/aenm.201702348

Cheng, X.-B., Zhao, C.-Z., Yao, Y.-X., Liu, H., and Zhang, Q. (2019). Recent advances in energy chemistry between solid-state electrolyte and safe lithium-metal anodes. *Inside Chem.* 5 (1), 74–96. doi:10.1016/j.chempr.2018.12.002

Deiseroth, H. J., Kong, S. T., Eckert, H., Vannahme, J., Reiner, C., Zaiss, T., et al. (2008). Li6PS5X: a class of crystalline Li-rich solids with an unusually high Li+ mobility. *Angew Chem. Int. Ed. Engl.* 47 (4), 755–758. doi:10.1002/ange.200703900

Deng, Y., Eames, C., Chotard, J. N., Lalère, F., Seznec, V., Emge, S., et al. (2015). Structural and mechanistic insights into fast lithium-ion conduction in Li4SiO4-Li3PO4 solid electrolytes. *J. Am. Chem. Soc.* 137 (28), 9136. doi:10.1021/jacs.5b04444

Ding, B., Wang, J., Fan, Z., Chen, S., Lin, Q., Lu, X., et al. (2020). Solid-state lithium-sulfur batteries: advances, challenges and perspectives. *Mater. Today* 40, 114–131. doi:10.1016/j.mattod.2020.05.020

Fan, L., Wei, S., Li, S., Li, Q., and Lu, Y. (2018). Recent progress of the solid-state electrolytes for high-energy metal-based batteries. *Adv. Energy Mater.* 8 (11), 1702657. doi:10.1002/aenm.201702657

Geng, P., Cao, S., Guo, X., Ding, J., Zhang, S., Zheng, M., et al. (2019). Polypyrrole coated hollow metal-organic framework composites for lithium-sulfur batteries. *J. Mater. Chem.* 7 (33), 19465–19470. doi:10.1039/C9TA05812E

Guo, J., Xu, Y., and Wang, C. (2011). Sulfur-impregnated disordered carbon nanotubes cathode for lithium-sulfur batteries. *Nano Lett.* 11 (10), 4288–4294. doi:10.1021/nl202297p

Han, F., Yue, J., Fan, X., Gao, T., Luo, C., Ma, Z., et al. (2016a). High-performance all-solid-state lithium-sulfur battery enabled by a mixed-conductive Li2S nanocomposite. *Nano Lett.* 16 (7), 4521–4527. doi:10.1021/acs.nanolett.6b01754

Han, F., Zhu, Y., He, X., Mo, Y., and Wang, C. (2016b). Electrochemical stability of Li10 GeP2 S12 and Li7 La3 Zr2 O12 solid electrolytes. *Adv. Energy Mater.* 6 (8), 1501590. doi:10.1002/aenm.201501590

Han, X., Xu, Y., Chen, X., Chen, Y.-C., Weadock, N., Wan, J., et al. (2013). Reactivation of dissolved polysulfides in Li-S batteries based on atomic layer deposition of Al2O3 in nanoporous carbon cloth. *Nanomater. Energy* 2 (6), 1197–1206. doi:10.1016/j.nanoen.2013.05.003

Han, X.-R., Guo, X.-T., Xu, M.-J., Pang, H., and Ma, Y.-W. (2020). Clean utilization of palm kernel shell: sustainable and naturally heteroatom-doped porous activated carbon for lithium-sulfur batteries. *Rare Met.* 39 (9), 1099–1106. doi:10.1007/s12598-020-01439-9

Huang, B., Yao, X., Huang, Z., Guan, Y., Jin, Y., and Xu, X. (2015). Li 3 PO 4 -doped Li 7 P 3 S 11 glass-ceramic electrolytes with enhanced lithium ion conductivities and application in all-solid-state batteries. *J. Power Sources* 284, 206–211. doi:10.1016/j.jpowsour.2015.02.160

Jayaprakash, N., Shen, J., Moganty, S. S., Corona, A., and Archer, L. A. (2011). Porous hollow carbon@sulfur composites for high-power lithium-sulfur batteries. *Angew Chem. Int. Ed. Engl.* 50 (26), 5904–5908. doi:10.1002/anie.201100637

Ji, X., Lee, K. T., and Nazar, L. F. (2009). A highly ordered nanostructured carbon-sulphur cathode for lithium-sulphur batteries. *Nat. Mater.* 8 (6), 500–506. doi:10.1038/nmat2460

Kamaya, N., Homma, K., Yamakawa, Y., Hirayama, M., Kanno, R., Yonemura, M., et al. (2011). A lithium superionic conductor. *Nat. Mater.* 10 (9), 682–686. doi:10.1038/nmat3066

Kanno, R., and Murayama, M. (2001). Lithium ionic conductor thio-LISICON: the Li[sub 2]S-GeS[sub 2]-P[sub 2]S[sub 5] system. *J. Electrochem. Soc.* 148 (7), A742. doi:10.1149/1.1379028

Kato, Y., Hori, S., Saito, T., Suzuki, K., Hirayama, M., Mitsui, A., et al. (2016). High-power all-solid-state batteries using sulfide superionic conductors. *Nat Energy* 1 (4), 16030. doi:10.1038/nenergy.2016.30

Liang, X., Hart, C., Pang, Q., Garsuch, A., Weiss, T., and Nazar, L. F. (2015). A highly efficient polysulfide mediator for lithium-sulfur batteries. *Nat. Commun.* 6 (1), 5682. doi:10.1038/ncomms6682

Lin, Z., Liu, Z., Dudney, N. J., and Liang, C. (2013). Lithium superionic sulfide cathode for all-solid lithium-sulfur batteries. *ACS Nano.* 7 (3), 2829–2833. doi:10.1021/nn400391h

Liu, Z., Fu, W., Payzant, E. A., Yu, X., Wu, Z., Dudney, N. J., et al. (2013). Anomalous high ionic conductivity of nanoporous β-Li3PS4. *J. Am. Chem. Soc.* 135 (3), 975–978. doi:10.1021/ja3110895

Liu, W., Liu, N., Sun, J., Hsu, P. C., Li, Y., Lee, H. W., et al. (2015). Ionic conductivity enhancement of polymer electrolytes with ceramic nanowire fillers. *Nano Lett.* 15 (4), 2740–2745. doi:10.1021/acs.nanolett.5b00600

Liu, T., Zhang, Y., Zhang, X., Wang, L., Zhao, S.-X., Lin, Y.-H., et al. (2018). Enhanced electrochemical performance of bulk type oxide ceramic lithium batteries enabled by interface modification. *J. Mater. Chem.* 6 (11), 4649–4657. doi:10.1039/C7TA06833F

Liu, C., Bai, Y., Zhao, Y., Yao, H., and Pang, H. (2020). MoS2/graphene composites: fabrication and electrochemical energy storage. *Energy Storage Materials* 33, 470–502. doi:10.1016/j.ensm.2020.06.020

Lochala, J., Liu, D., Wu, B., Robinson, C., and Xiao, J. (2017). Research progress toward the practical applications of lithium-sulfur batteries. *ACS Appl. Mater. Interfaces* 9 (29), 24407–24421. doi:10.1021/acsami.7b06208

Ma, Z., Xue, H.-G., and Guo, S.-P. (2018). Recent achievements on sulfide-type solid electrolytes: crystal structures and electrochemical performance. *J. Mater. Sci.* 53 (6), 3927–3938. doi:10.1007/s10853-017-1827-6

Nitta, N., Wu, F., Lee, J. T., and Yushin, G. (2015). Li-ion battery materials: present and future. *Mater. Today* 18 (5), 252–264. doi:10.1016/j.mattod.2014.10.040

Ohara, K., Mitsui, A., Mori, M., Onodera, Y., Shiotani, S., Koyama, Y., et al. (2016). Structural and electronic features of binary Li2S-P2S5 glasses. *Sci. Rep.* 6, 21302. doi:10.1038/srep21302

Ohno, S., Koerver, R., Dewald, G., Rosenbach, C., Titscher, P., Steckermeier, D., et al. (2019). Observation of chemomechanical failure and the influence of cutoff potentials in all-solid-state Li-S batteries. *Chem. Mater.* 31 (8), 2930–2940. doi:10.1021/acs.chemmater.9b00282

Ohtomo, T., Hayashi, A., Tatsumisago, M., Tsuchida, Y., Hama, S., and Kawamoto, K. (2013). All-solid-state lithium secondary batteries using the 75Li2S·25P2S5 glass and the 70Li2S·30P2S5 glass-ceramic as solid electrolytes. *J. Power Sources* 233, 231–235. doi:10.1016/j.jpowsour.2013.01.090

Pang, Q., Liang, X., Kwok, C. Y., and Nazar, L. F. (2016). Advances in lithium-sulfur batteries based on multifunctional cathodes and electrolytes. *Nat Energy* 1 (9), 16132. doi:10.1038/nenergy.2016.132

Qu, H., Zhang, J., Du, A., Chen, B., Chai, J., Xue, N., et al. (2018). Multifunctional sandwich-structured electrolyte for high-performance lithium-sulfur batteries. *Adv. Sci.* 5 (3), 1700503. doi:10.1002/advs.201700503

Sakuma, M., Suzuki, K., Hirayama, M., and Kanno, R. (2016). Reactions at the electrode/electrolyte interface of all-solid-state lithium batteries incorporating Li-M (M = Sn, Si) alloy electrodes and sulfide-based solid electrolytes. *Solid State Ionics* 285, 101–105. doi:10.1016/j.ssi.2015.07.010

Seino, Y., Ota, T., Takada, K., Hayashi, A., and Tatsumisago, M. (2014). A sulphide lithium super ion conductor is superior to liquid ion conductors for use in rechargeable batteries. *Energy Environ. Sci.* 7 (2), 627–631. doi:10.1039/C3EE41655K

Shen, X., Cheng, X., Shi, P., Huang, J., Zhang, X., Yan, C., et al. (2019). Lithium-matrix composite anode protected by a solid electrolyte layer for stable lithium metal batteries. *Journal of Energy Chemistry* 37, 29–34. doi:10.1016/j.jechem.2018.11.016

Takada, K., Ohta, N., and Tateyama, Y. (2015). Recent progress in interfacial nanoarchitectonics in solid-state batteries. *J. Inorg. Organomet. Polym.* 25 (2), 205–213. doi:10.1007/s10904-014-0127-8

Takeuchi, T., Kageyama, H., Nakanishi, K., Tabuchi, M., Sakaebe, H., Ohta, T., et al. (2010). All-solid-state lithium secondary battery with Li[sub 2]S-C composite positive electrode prepared by spark-plasma-sintering process. *J. Electrochem. Soc.* 157 (11), A1196. doi:10.1149/1.3486083

Wang, H., Yang, Y., Liang, Y., Robinson, J. T., Li, Y., Jackson, A., et al. (2011). Graphene-wrapped sulfur particles as a rechargeable lithium-sulfur battery cathode material with high capacity and cycling stability. *Nano Lett.* 11 (7), 2644–2647. doi:10.1021/nl200658a

Wang, S., Zhang, Y., Zhang, X., Liu, T., Lin, Y.-H., Shen, Y., et al. (2018a). High-conductivity argyrodite Li6PS5Cl solid electrolytes prepared via optimized sintering processes for all-solid-state lithium-sulfur batteries. *ACS Appl. Mater. Interfaces* 10 (49), 42279–42285. doi:10.1021/acsami.8b15121

Wang, X., Zhang, Y., Zhang, X., Liu, T., Lin, Y.-H., Li, L., et al. (2018b). Lithium-salt-rich PEO/Li0.3La0.557TiO3 interpenetrating composite electrolyte with three-dimensional ceramic nano-backbone for all-solid-state lithium-ion batteries. *ACS Appl. Mater. Interfaces* 10 (29), 24791–24798. doi:10.1021/acsami.8b06658

Wei Seh, Z., Li, W., Cha, J. J., Zheng, G., Yang, Y., McDowell, M. T., et al. (2013). Sulphur-TiO2 yolk-shell nanoarchitecture with internal void space for long-cycle lithium-sulphur batteries. *Nat. Commun.* 4 (1), 1331. doi:10.1038/ncomms2327

Wenzel, S., Randau, S., Leichtweiß, T., Weber, D. A., Sann, J., Zeier, W. G., et al. (2016a). Direct observation of the interfacial instability of the fast ionic conductor Li10GeP2S12 at the lithium metal anode. *Chem. Mater.* 28 (7), 2400–2407. doi:10.1021/acs.chemmater.6b00610

Wenzel, S., Weber, D. A., Leichtweiss, T., Busche, M. R., Sann, J., and Janek, J. (2016b). Interphase formation and degradation of charge transfer kinetics between a lithium metal anode and highly crystalline Li7P3S11 solid electrolyte. *Solid State Ionics* 286, 24–33. doi:10.1016/j.ssi.2015.11.034

Wenzel, S., Sedlmaier, S. J., Dietrich, C., Zeier, W. G., and Janek, J. (2018). Interfacial reactivity and interphase growth of argyrodite solid electrolytes at lithium metal electrodes. *Solid State Ionics* 318, 102–112. doi:10.1016/j.ssi.2017.07.005

Yan, M., Wang, W.-P., Yin, Y.-X., Wan, L.-J., and Guo, Y.-G. (2019). Interfacial design for lithium-sulfur batteries: from liquid to solid. *Energy* 1 (1), 100002. doi:10.1016/j.enchem.2019.100002

Yin, Y. X., Xin, S., Guo, Y. G., and Wan, L. J. (2013). Lithium-sulfur batteries: electrochemistry, materials, and prospects. *Angew Chem. Int. Ed. Engl.* 52 (50), 13186–13200. doi:10.1002/anie.201304762

Yu, C., van Eijck, L., Ganapathy, S., and Wagemaker, M. (2016). Synthesis, structure and electrochemical performance of the argyrodite Li 6 PS 5 Cl solid electrolyte for Li-ion solid state batteries. *Electrochim. Acta* 215, 93–99. doi:10.1016/j.electacta.2016.08.081

Yubuchi, S., Teragawa, S., Aso, K., Tadanaga, K., Hayashi, A., and Tatsumisago, M. (2015). Preparation of high lithium-ion conducting Li6PS5Cl solid electrolyte from ethanol solution for all-solid-state lithium batteries. *J. Power Sources* 293, 941–945. doi:10.1016/j.jpowsour.2015.05.093

Zhang, C., Lin, Y., and Liu, J. (2015). Sulfur double locked by a macro-structural cathode and a solid polymer electrolyte for lithium-sulfur batteries. *J. Mater. Chem.* 3 (20), 10760–10766. doi:10.1039/C5TA01037C

Zhang, J., Shi, Y., Ding, Y., Zhang, W., and Yu, G. (2016). *In Situ* reactive synthesis of polypyrrole-MnO2 coaxial nanotubes as sulfur hosts for high-performance lithium–sulfur battery. *Nano Lett.* 16 (11), 7276–7281. doi:10.1021/acs.nanolett.6b03849

Zhang, Y., Chen, R., Liu, T., Shen, Y., Lin, Y., and Nan, C.-W. (2017). High capacity, superior cyclic performances in all-solid-state lithium-ion batteries based on 78Li2S-22P2S5 glass-ceramic electrolytes prepared via simple heat treatment. *ACS Appl. Mater. Interfaces* 9 (34), 28542–28548. doi:10.1021/acsami.7b06038

Zhang, J., Zhong, H., Zheng, C., Xia, Y., Liang, C., Huang, H., et al. (2018a). All-solid-state batteries with slurry coated LiNi0.8Co0.1Mn0.1O2 composite cathode and Li6PS5Cl electrolyte: effect of binder content. *J. Power Sources* 391, 73–79. doi:10.1016/j.jpowsour.2018.04.069

Zhang, Y., Chen, R., Liu, T., Xu, B., Zhang, X., Li, L., et al. (2018b). High capacity and superior cyclic performances of all-solid-state lithium batteries enabled by a glass-ceramics solo. *ACS Appl. Mater. Interfaces* 10 (12), 10029–10035. doi:10.1021/acsami.7b18211

Zhang, J., Zheng, C., Lou, J., Xia, Y., Liang, C., Huang, H., et al. (2019). Poly(ethylene oxide) reinforced Li6PS5Cl composite solid electrolyte for all-solid-state lithium battery: enhanced electrochemical performance, mechanical property and interfacial stability. *J. Power Sources* 412, 78–85. doi:10.1016/j.jpowsour.2018.11.036

Zhang, J., Zheng, C., Li, L., Xia, Y., Huang, H., Gan, Y., et al. (2020). Unraveling the intra and intercycle interfacial evolution of Li6PS5Cl-based all-solid-state lithium batteries. *Advanced Energy Materials* 10 (4), 1903311. doi:10.1002/aenm.201903311

Zhang, Z., and Kennedy, J. (1990). Synthesis and characterization of the B2S3 Li2S, the P2S5 Li2S and the B2S3 P2S5 Li2S glass systems. *Solid State Ionics* 38(3), 217–224. doi:10.1016/0167-2738(90)90424-p

Zhao, E., Wang, J., Li, F., Jiang, Z., Yang, X. Q., Wang, F., et al. (2019). Exploring reaction dynamics in lithium-sulfur batteries by time-resolved operando sulfur K-edge X-ray absorption spectroscopy. *Chem. Commun.* 55 (34), 4993–4996. doi:10.1039/C9CC00485H

Zhao, C.-Z., Zhao, B.-C., Yan, C., Zhang, X.-Q., Huang, J.-Q., Mo, Y., et al. (2020). Liquid phase therapy to solid electrolyte-electrode interface in solid-state Li metal batteries: a review. *Energy Storage Materials* 24, 75–84. doi:10.1016/j.ensm.2019.07.026

Zheng, C., Niu, S., Lv, W., Zhou, G., Li, J., Fan, S., et al. (2017). Propelling polysulfides transformation for high-rate and long-life lithium-sulfur batteries. *Nanomater. Energy* 33, 306–312. doi:10.1016/j.nanoen.2017.01.040

Zheng, M., Chi, Y., Hu, Q., Tang, H., Jiang, X., Zhang, L., et al. (2019). Carbon nanotube-based materials for lithium-sulfur batteries. *J. Mater. Chem.* 7 (29), 17204–17241. doi:10.1039/C9TA05347F

Zhu, Y., He, X., and Mo, Y. (2015). Origin of outstanding stability in the lithium solid electrolyte materials: insights from thermodynamic analyses based on first-principles calculations. *ACS Appl. Mater. Interfaces* 7 (42), 23685–23693. doi:10.1021/acsami.5b07517

Zhu, Y., He, X., and Mo, Y. (2016). First principles study on electrochemical and chemical stability of solid electrolyte-electrode interfaces in all-solid-state Li-ion batteries. *J. Mater. Chem.* 4 (9), 3253–3266. doi:10.1039/C5TA08574H

Conflict of Interest: The authors declare that the research was conducted in the absence of any commercial or financial relationships that could be construed as a potential conflict of interest.